Polycrystalline Metal Strength at Tension.

Author: Boris Nudelman

Affiliation: Boris Nudelman Engineering, Technology Functional analysis, Self-

employed.

Company site: https://nudelmanengineerin.wixsite.com/nudelmanengineering

Address: Nativ Hamazalot st. 21/4, Jerusalem, postcode 9783021, Israel

Correspondence to: Boris Nudelman (nudelmanengineering@gmail.com)

ORCID: 0000-0002-6450-6153

1. First statement.

The present paper includes some preliminary steps before Experimental Research Program of the metal strength at tension, should be performed.

2. Introduction.

The physical mechanism of the plastic strain of metal single crystals was considered in the first article of this project [1]. Despite proved similarity the mechanism of polycrystals differ of it. It caused by difference in structure. Besides, analysis of [1] was made with arbitrary assumptions, have been specified here as possible. In accordance to [1] the first stage of hardening is characterized of follow attributes: 1) the flow occurs in transverse direction relative to the tension axis and begins from the surface; 2) the plastic flow beginning – elastic limit is consider as strong increasing of the probability of the single penetration acts of the surface unstable atoms into internal specimen space; 3) the single act zone arbitrary restricted; 4) the plastic flow speed dependence of time assumed; 5) the displacement of the internal atoms not taken in account in mass transfer

1

balance. Moreover, it's rational to consider the properties of the object, which traditionally are applied without strong physical ground.

3. Definition and properties of the object should be analyzed.

The tensile test process of metal specimens is considered. The specimen shapes and dimensions specified inherent in the macro scale material properties. As sample, flat and round specimens (dog bone shaped). Cross section dimensions: thickness – h, width – b limited as ~1...25mm; diameter d=1...25mm; length of strain gauge part $l \ge 5b$, ($l \ge 5d$). Pronounced differs from single crystals – poly crystal structure and surface roughness. The strength dependence of structure, particularly on the grain size and other metallurgical factors, studied well, [2,3]. It not consider here. The known confirmed strength dependence on surface roughness [4,5,6,7,8], required certain analysis. In sight of [1] the plastic strain begins from the surface. To get a comparable analysis result, the quasistatic loading process is considered. The last defined as the relative strain speed restriction, $\dot{\varepsilon}$. In accordance with several sources, [9], not over of conventional, about: $\dot{\varepsilon}_s \le 10^{-4} \frac{1}{s}$.

- 4. Strength dependence on the specimen surface roughness.
- 4.1 The model definition.

Typical kinds of surface roughness schematically presented in Fig 1. Consequently: a – periodical alternation of the ledges and notches; b -serrated curve, superimposed on wave line of tracing of processing; c – serrating curve a small amplitude, as sequence of high-quality treatment.

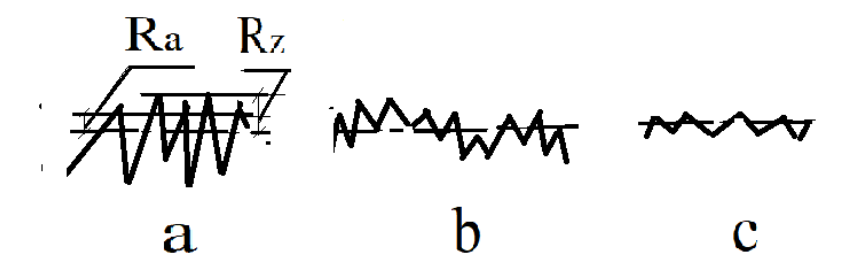


Fig.1: Types of surface roughness.

The peak heights of roughness, Rp, their exist in all types of profilers. Frequently they exceed the RMS value, Ra, (as $\sim 2...3$ times) and amplitude values, Rz. Naturally, the peak values have been considered for strength appraisal. Mostly they are observed in a diagrams of type b. Two variants of roughness distribution are consider in Fig.2: a - periodical alternation of the ledges and notches with peak (the longitudinal scale of profile diagram [7, p.5,fig5] is reproduced); b – extended along tension axis displacement of peak notches, (the longitudinal scale of profile diagram [4, p.4,fig.3a] is reproduced).

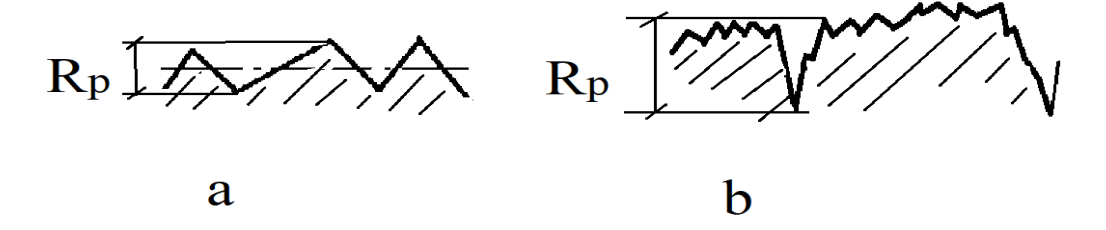


Fig.2 Two types of peak roughness distribution.

Possible shape and orientation of ledge and notch are considered, Fig.3, a, b. They are symmetrical relative to tension axis and extended in transverse direction.

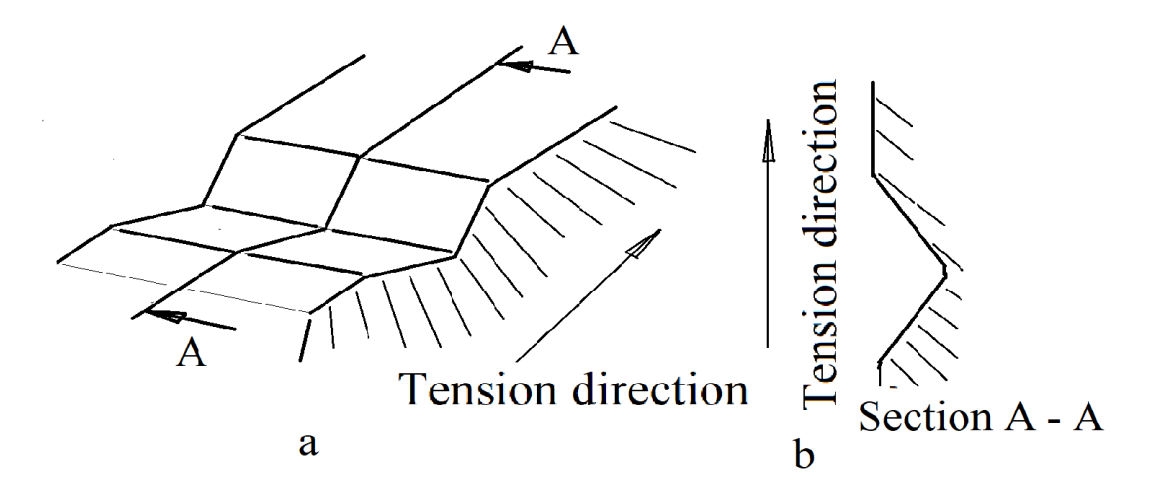


Fig. 3 Accepted ledge shape and orientation.

4.2 Ledges effect.

The ledge peak height, $Rp = 4.5\mu m$, has chosen. It meets a medium quality of treatment relations, $Ra = 1.5\mu m$. Accordingly, to conventional point of view, their exist a uniform stress field in each specimen cross section at loading:

$$\sigma_z = \sigma_{un} = Const$$

Actually, uniform field distorted in a ledge zone. Partial load decreasing of nearest volume occurs due to the stresses into the ledge volume, Fig.4, a. Ledge dimensions chosen intentionally to avoid doubt of material macro properties may be applied. First, continuity and isotropy. In addition, the ledge shape and place relative to the longitude section axis of symmetry allows to define the stress- strain state as flat. Special analysis is required for the quantitative appraisal of the stress field in the ledge area. However, in consequence of it, local distortion of flat sections occurs. The scheme of distortion shown in Fig.4, b.

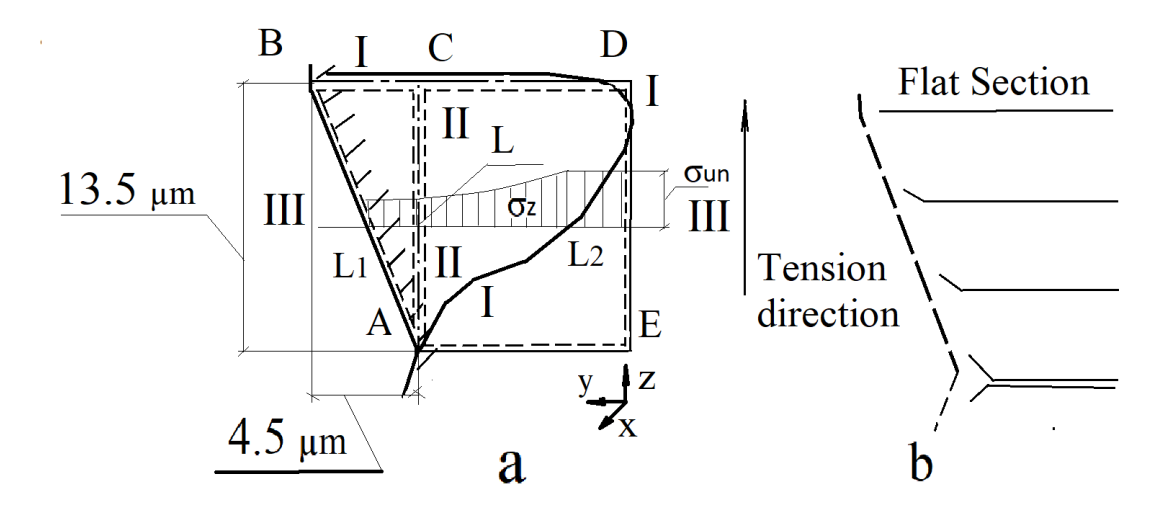


Fig.4 a – ledge geometry and load diagram; b – cross section deplanation scheme.

The boundary of the uniform stress field, Fig.4 a, by continuous line I-I-I is shown. Dash slotted line II-II defined the boundary with relation of ledge absence. The equilibrium of both sides II-II in any transverse section III-III in the ledge zone:

$$\int_{y_L}^{y_{L2}} \sigma_z \cdot dy = \int_{y_L}^{y_{L1}} \sigma_{un} (1 - \sigma_z) \cdot dy . \tag{1}$$

In [1] the model of linear stress state was used, because of in other directions (x and y) active forces are absent. The design scheme of two pieces in longitude section of ledge may to consider. First – triangled ledge profile from

bottom of notch, point A, till top, p. B; from B to C by horizontal line, continue of line I-I. Second – rectangular, restricted by lines: AC; CD; DE; EA, where AC – the border with first piece. CD and DE are fully defined of the ledge influence zone. Pieces areas are F1 and F2. Directly from (1):

$$\iint_{F_1} \sigma_z \times dy \times dz = l_{CD} \times l_{DE} \times \sigma_{un} - \iint_{F_2} \sigma_z \times dy \times dz . \quad (2)$$

The physical sense of (2) may be defined with dividing it both parts to the modulus of elasticity – E. Both parts of the (2) are turning to the integral sums of displacement of each part. The displacement diagram shown in Fig. 5, a.

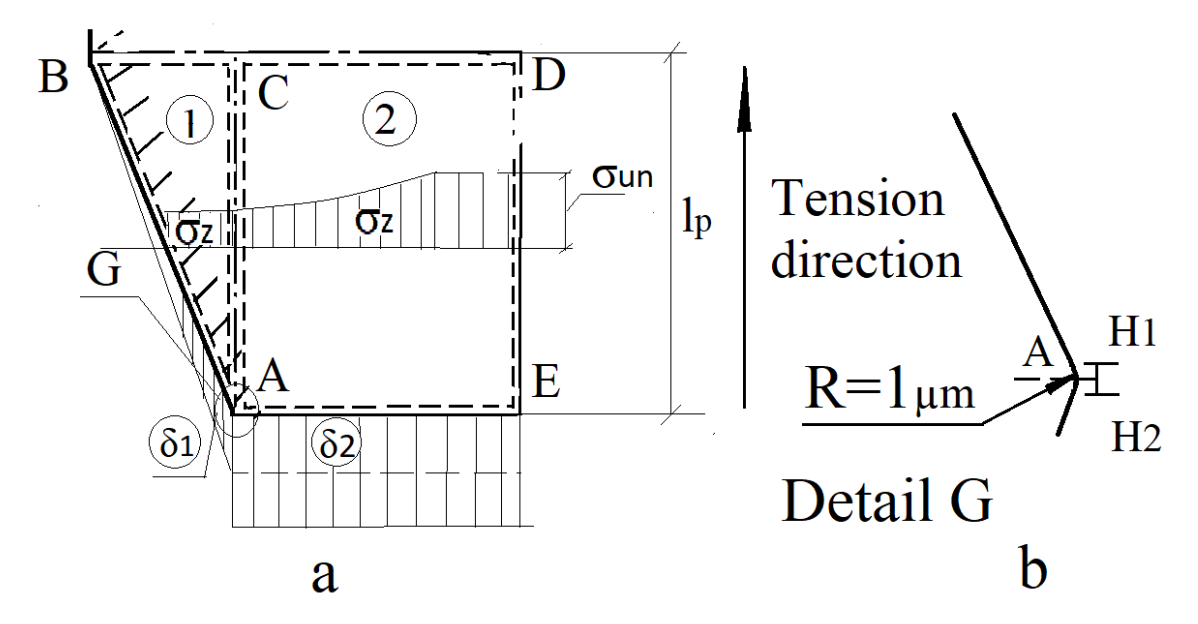


Fig. 5; a – Two parts of ledge region, displacement diagram; b – notch geometry.

Approximate stress diagram of any section shown there also. The stresses in the ledge zone are decreased from the σ_{un} to an undefined value on the surface. The stress distribution function is statically indeterminate problem. Moreover, the same as in [1], it may not to apply the general elastic low ratios, even for flat stress state form. As signed in [1], the general low includes physically incorrect assumption: 1) superposition principal and 2) continuity

violation, in stress components definition. Nonetheless, the theory shortcomings do not make impossible to apprise a solution with an engineer method. The physically grounded law of stress gradient required for such appraisal. Hence, non-conventional method should be applied. The virtual model of two pats, I and II, which are disconnected along border AC (dashed lines), Fig.5, is consider. First part is under the uniform stresses σ_{un} , which act along BC. It's accepted that they are decreased along border AC to zero at p. A. This relation inserted to compensate real stresses, acts along BC. As consequence of first part geometry, it's largest part of the area is loaded of a big values stress. It comparts the stress low difference of ledge height - $BC = R_p = 4.5 \mu m$. So: $\sigma_z(z) = \frac{\sigma_{un}}{l_0} \times z$. (3)

Hence, the "stresses sum" depends on the ledge area F1. This meets physical relations. Stress distribution in any transverse section, Fig.5 with approximation: $\sigma_z(y) = Const$. With all assumptions:

$$\int_{F_1} \sigma_z = \int_0^{l_p} \left(\frac{\sigma_{un}}{l_p} \right) \times z \times \left(\frac{R_p}{l_p} \right) \times z \times dz = \frac{\sigma_{un} \times R_p}{l_p^2} \int_0^{l_p} z^2 \times dz =$$

$$\frac{\sigma_{un} \times R_p}{l_p^2} \times \frac{l_p^3}{3} = \frac{\sigma_{un} \times R_p \times l_p}{3} = \frac{2 \times \sigma_{un}}{3} \times \left(\frac{R_p \times l_p}{2} \right) . \quad (4)$$

It's appropriate here to formulate the statement, may be presented as theorem: - In elastic state the integral sum of displacements in a region (linear or flat) is invariant of stresses distribution with relation of constant stresses integral sum. The stresses sum may be defined as stress average value multiplied the region area (4). From last, the resulted "displacement" along the border AC:

$$U_{AC1} = \frac{2 \times \sigma_{un}}{3} \times l_p . \tag{5}$$

The virtually disconnected part 2, F2, with uniform field - σ_{un} is loaded. In the same way, the resulted "displacement" along the border AC:

$$U_{AC2} = \sigma_{un} \times l_p . (6)$$

Real, non-virtual "displacement" appraisal assumed as average value:

$$U_{AC} = \frac{U_{AC1} + U_{AC2}}{2} = \frac{5}{6} \sigma_{un} \times l_p ,$$
 (7)

From (7) full deplanation for the considered sample: $\delta u_{AE} = \frac{1}{E} (U_{AC2} - U_{AC}) = \frac{1}{6} \times 13.5 \mu m \times \varepsilon_{un} = 2.25 \times \varepsilon_{un} \mu m$. (8)

In sight of all assumptions, (8) may be accounted as approximation only.

4.3 Notches effect.

The notch shape is presented in Fig.5 b, detail G. As regards to stress-strain state, the notch bottom radius is critical. However, it may not be defined from roughness diagram. It assumed as in [4] - 1 μm . It's also proposed, that neither author nor reader never held the reference books with stress concentrator tables and not saw once moire stripes around concentrator in the photo elasticity stage. The strain of straightened line segment AH1 is considered. It's length - 0.5 μm , Fig.5, b. The strain with a low error (caused by resistance) is equal to bottom line (AE) deplanation. The value:

$$\varepsilon_{AH1} = \frac{2.25 \times \varepsilon_{un}}{0.5} = 4.5 \times \varepsilon_{un} ; \qquad (9)$$

Hence, plastic strain wills start at: $\varepsilon_{un} = \frac{\varepsilon_e}{4.5}$. (9) may be accounted for physical ground of the microplasticity effect.

4.3.1. Strain at the quasistatic loading.

For the considered sample the specimen loading till the elastic limit, $\varepsilon_{un} = \varepsilon_e$, cause the 4.5 time relaxation, (unloading) of AH segment of notch bottom. The material plastic properties influence on it famously. For example, for ductile steel

with elastic limit $\varepsilon_e=0.1\dots0.15$ %, full relative strain will reach $\varepsilon_n\leq0.675$ %, which is more less than yielding plateau: $\varepsilon_{pl}\approx1.2\dots2.3$ %. This mean that loading manner will not change till load maximum - σ_u . At a repeated cycle, even in the elastic state the microplasticity accumulation must occur – plastic strain spread from the surface into the specimen volume. The spread mechanism by Bauschinger effect is defined. It shortly considered in [1].

4.3.2 The strain in pulsating cycle.

Pulsating cycle, tension – unloading mostly is dynamic one. That's why the plastic part of strain decreasing is possible. It occurs because of the restriction of yielding strain rate. In another side, the elastic strain waves have been included into account. In a modern publication, so called, Kolsky Waves [10] The variants of resonance maximums and minimums may occur. The lasts may falsify the fatigue tests.

4.3.3 The strain at the symmetric cycle.

Symmetric cycle of loading is specific for fatigue material tests. The notch effect influence is typical in this case. Typically, the search by topic "strength – surface roughness" gives almost fatigue publications only. Stress diagrams of bottom section by cycle elements in Fig. 6 are considered. The appraisal fulfilled with dynamic component but without waves influence.

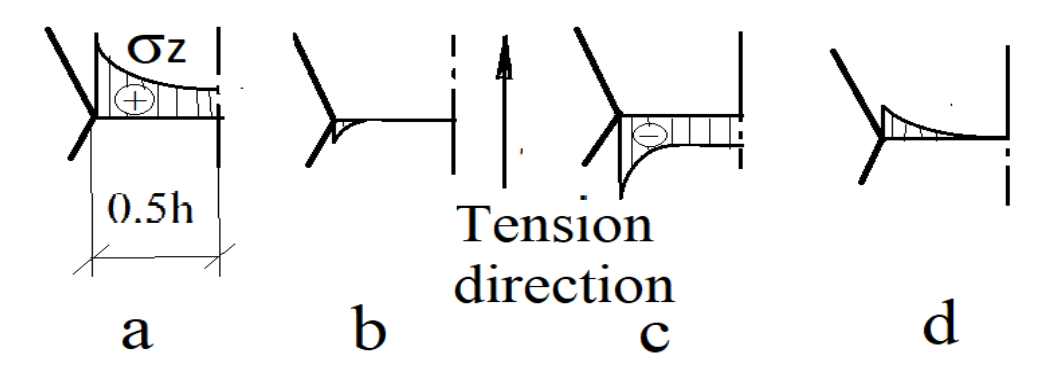


Fig. 6 Notch stress diagrams of the symmetric loading cycle: a – tension element; b – unloading; c – compression; d – unloading.

The diagram of the tension element shown in Fig.6 a. Whole section loaded with $\sigma_z = \sigma_{un}$. The surface stresses (bottoms of roughness) exceeds this value. In the considered sample with strain average rate - $\dot{\varepsilon}_s = 10^{-2}~s^{-1}$; the loading level - $\sigma_{un} = 0.5\sigma_e$; $\varepsilon_{un} = 0.5\varepsilon_e$; loading time - $t_{0.5s} = \frac{0.5\varepsilon_e}{\dot{\varepsilon}_s} = 0.5\times0.0015/10^{-2} = 0.075~s$; from (9) strain rate of the segment AH1: $\varepsilon_{AH1} = 4.5\times\dot{\varepsilon}_s = 4.5\times10^{-2}~s^{-1} = 0.045~s^{-1}$. This value is approximately equal to average one of two analogues: : [11,p.4, Fig.2], where $\dot{\varepsilon}_1 = 0.09~s^{-1}$, yielding hump $\sigma_{1H} \approx 1.5\sigma_e$; [12,p.3,Fig.1], where $\varepsilon_2 = 9.09\times10^{-4}~s^{-1}$, yielding hump $\sigma_{2H} \approx 1.0.3\sigma_e$. The maximal stress: $\sigma_{AH1} \approx 2.25\sigma_e$. The strain plastic component here is minimal, because of unloading follow almost instantly. The process occurs in a micro scale. That's why the analogue with single crystal may be rational [ref.1], where proportionality lasts till rather large load. In accordance with it, the Bauschinger effect does not appear. So, dynamic fatigue tests may be incorrect for material long-term strength appraisal of the quasi-static loading.

5 The plastic strain model.

5.2 Plastic strain at the first stage hardening.

The attributes of plastic flow model of single crystal [1] signed in introduction. The first of it, the transverse plastic strain direction is confirmed by the follow articles of this project. The elastic limit definition does not contradict to the known experimental data. It is defined as beginning of plural penetration acts of surface atoms into a specimen space. As regard to the samples of single crystal loading, [1], it's rational to sign their features. The loading diagram of metal crystal as linear growth till maximum and fast unloading to the yield stress. The

such diagram type is defined by surface defect absence and mostly by micron sized cross section. In accordance to [11], it may be explained that the "Delay Yield Phenomenon" is existed and contemporary plural penetration acts of surface atoms occur. Wherein, formation of the surface deformed layer is impossible due to the ratio of its volume to common one is about 1. The zone of influence in [1] were arbitrary chosen. As regards to the poly crystal specimens of macro scale, their exist data for the clearer model of the process. The beginning, the exit of surface atoms from equilibrium is the same as for single crystals. Respectively, the proportionality limit definition is the same also. Here is worth to refer the mechanistic model, proposed in [13]. The yielding delay was experimentally detected in [11]. It seems necessary and sufficient cause of yielding hump appearance in the loading diagram of ductile metals. A number of results of similar experiments make possible to correct the temporal characteristic of yield beginning. The whole diagram first part has the lowest tape to strain axis. With it, the strain grows uniformly. It allows to consider the process as two independence ones. First – increased elastic. Second – irreversible plastic. In case horizontal diagram line – the load does not grow. Plateau. Last mean that elastic fully compensates by plastic:

$$\Delta \varepsilon_e = \Delta \varepsilon_n \tag{10}$$

Here $\Delta \varepsilon_p$ – plastic strain increment, as accumulation of surface atoms penetration acts. It's rational redefine the zone of influence, dispersion in specimen space of the plastic strain. As in most physical processes of equilibration – exponential decreasing from local point on surface occur. As sequence of penetration acts accumulation, the near surface layer with a steady state form. It corresponds of the classic plasticity statement of maximal energy change with plastic flow. The nested strain field of the plural acts may forms decreased from a surface to inside the specimen. The process is characterized of the satiety effect, which leads to flow character change, to second stage hardening. The indirect confirmation of

the superficial flow in the first hardening stage is the Piobert-Luders's effect appearance in a flat specimen. From a lot of experiments, it's known that the effect stops contemporary with the end of first stage. In accordance with a physical relation the delay [11] may be caused by the penetration act itself. In other side, the subsequent one, the strain equilibration in the volume occurs with a sound speed. The factors the process depends on are follows: the load rate; size effect; alloy composition, structure. Besides, the heterogeneity of the metal properties has been taken in account. As example; in [11] for low carbon steel – high dependance on load speed, high plastic yield delay; in [14] for high strength alloy steel - low sensitivity to load speed; in [12] for aluminum alloy - the plastic strain till satiety depends on the surface area. They exit an experimental data, where first stage hardening is absence in diagram. Representation of the surface layer formation may be accounted for the plastic flow dependence (relation) on a ratio of surface value (the near surface layer volume) to the total specimen volume. This relation, revealed experimentally, was used by J. Weissmuller and his team [15,16] as a basic in metal microstructure research. A good example of such relation may be the Piobert – Luders effect. It observed on flat specimens (large ratio) and not observed on round macro specimens (lower ratio); - observed on round micro specimens (large ratio).

5.1 Numerical estimation.

The typical stress – strain diagram of tension test presented in Fig.7. Generally it consists of the follow stages: 1 – elastic loading till proportionality limit, linear part, σ_{eh} ; 2 – non linear part from σ_{eh} to the yielding hump top σ_h ; 3 – stresses drop to the yielding limit (low limit), σ_e ; 4 – the part of yielding, first stage hardening, Luders strain, Plateau from σ_e to σ_{eL} ; 5 – the resistance to plastic flow increasing till the maximal value σ_u , temporary resistance to failure, ultimate strength, second and third stages of hardening. The continue of loading does not make much sense because it relates to the specimen failure. The analyzed below samples may be used as illustration for methods to define the process parameters.

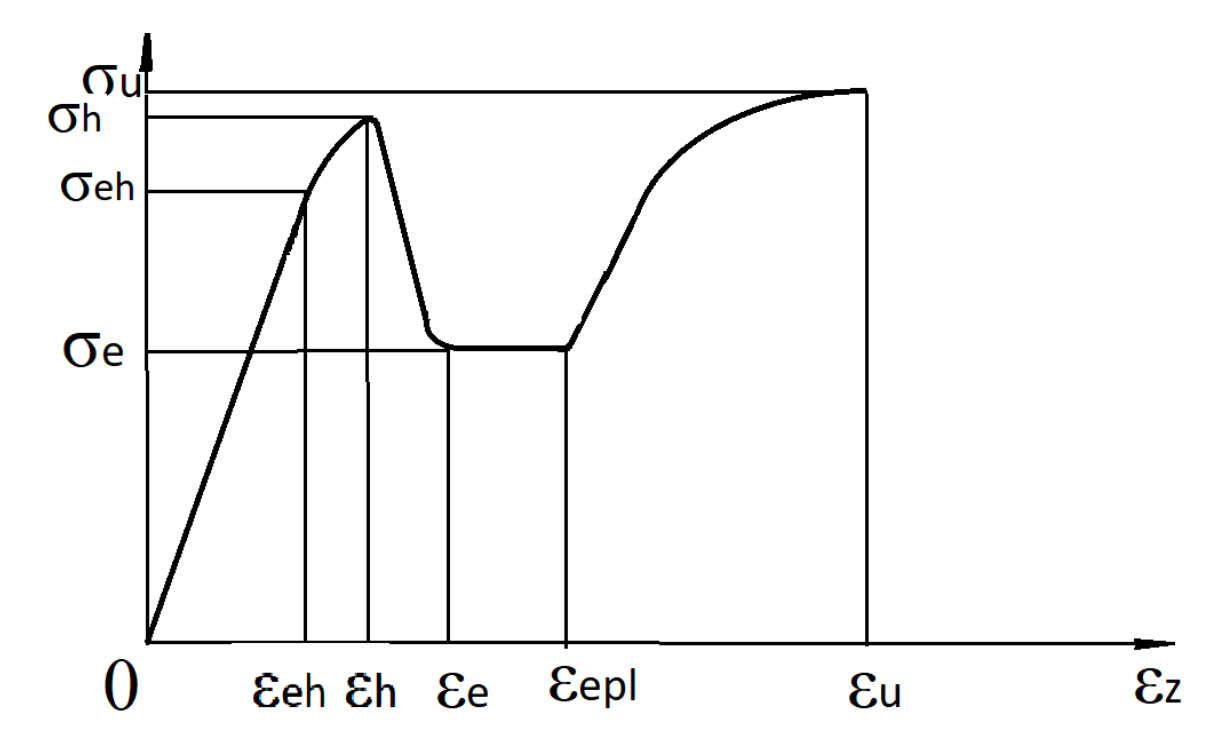


Fig.7 Typical tension stress – strain diagram.

First sample. The approximate data of [17Fig.1c] is used. The loading of the dual phase steel specimen, DP 600; cross section -1x4 mm: load rate - $\dot{\varepsilon}$ = 500 s^{-1} . The diagram linear part till point: $\sigma_{eh} = 780MPa$, $\varepsilon_{eh} = 4.6 \times 10^{-3}$ curved part till the hump top: $\sigma_H = 820MPa$, $\varepsilon_H = 5.3 \times 10^{-3}$. Stress drop till the proportional limit: $\sigma_e = 730MPa$, $\varepsilon_e = 0.0131$; Plateau: $\sigma_e = 730MPa$, $\varepsilon_{pl} = 0.015$.

The process dynamic characterization: the duration of yielding till hump top –

 $t_H = \frac{\varepsilon_H - \varepsilon_{eh}}{500} = \frac{(5.3 - 4.6) \times 10^{-3}}{500} = 1.4 \times 10^{-6} \ s \ ; \ \text{elastic component of the pressure}$ $\text{drop -} \Delta \sigma_0 = E \times \Delta \varepsilon = 2 \times 10^5 \times (5.3 - 4.6) \times 10^{-3} = 140 \ \textit{MPa} \ ; \ \text{plastic}$ $\text{component -} \ \varepsilon_{ph} = \frac{140 - 40}{E} = 5 \times 10^{-4} \ . \ \text{The yielding delay:}$

$$\Delta\varepsilon_e=\frac{\sigma_{eh}-\sigma_e}{E}=\frac{780-430}{2\times10^5}=0.00175 \quad \text{, время задержки (Yield}$$
 point delay): $\Delta t=\frac{1.75\times10^{-3}}{500}=0.35\times10^{-5}~s$.

Some notes for the last result clear understanding:

- 1) The theorem of invariant of the integral displacement is used here implicitly (as in part 4.2, p.4);
- 2) It's worth to fulfill the "Delay" quantitative determination with high load rate, but...
- 3) High speed requires the low differences values to be measured and processed, so...
- 4) It needs a high accuracy of measurements and a high stiffness of the system.
- 5) The delay independence on loading rate is not confirmed still.

Second sample. The approximate data of [14Fig.1] is used. The high strength alloyed steel (Fe,16.4Mn, 9.9Al, 0.86C-4.8Ni). Cross section dimensions: $1.3 \times 5 \ mm$; length- $10 \ mm$. Скорость - $\dot{\varepsilon} = 56 \ s^{-1}$. Elasticity modulus: $E = 2 \times 10^5 \ MPa$. Nonlinear part when load grows may not be defined in diagram. Hump stress - $\sigma_H = 1.31 \ GPa$; $\varepsilon_H = 0.01$. Horizontal part till, $\varepsilon_e = 0.0138$. Stress drop till proportionality limit:

$$\sigma_e = 1.285 \ GPa$$
 ; $\varepsilon_e = 0.0180$.

Total delay:
$$\Delta \varepsilon = \frac{\sigma_h - \sigma_e}{E} = \frac{1.31 - 1.285}{200} = 1.25 \times 10^{-4}$$
;

Delay duration:
$$\Delta t = \frac{\Delta \varepsilon}{\dot{\varepsilon}} = \frac{1.25 \times 10^{-4}}{56} = 2.2 \times 10^{-6} \text{ s}.$$

The last result is quite comparable with the first sample.

Third sample. The approximate data of [12, Fig.1] is used. Flat specimens – aluminum alloy 5456; cross section dimensions: width – 20mm; thickness – h = 1,-2,-3mm. Loading rate - - $\dot{\varepsilon}$ = 9.01 × 10⁻⁴ s⁻¹, close to quasi static. Elastic modulus - E = 0.705 MPa. Yielding hump does not appear in diagrams. Proportionality limit from loading diagram - σ_e = 150 MPa; ε_e = 0.002. Plateau (length) duration:

Specimen thick.
$$h_1 = 1 \text{mm} - \varepsilon_1 = 1.6 \times 10^{-2}$$
, on time $t_1 = 17.6 \, s$;
$$h_2 = 2 \text{mm} - \varepsilon_2 = 0.901 \times 10^{-2}$$
, on time $t_2 = 9.9 \, s$;
$$h_3 = 3 \text{mm} - \varepsilon_3 = 0.513 \times 10^{-2}$$
, on time $t_3 = 5.65 \, s$.

Plastic strain delay may not be defined because low strain speed. It's possible the only comparison of macro plastic strain component. The physical sense of the ε_i values in each plateau point is the by section summary relative strain. The flat sections are rightful in macro scale. ε_i in each point of section are equal and contains two components: plastic - ε_{pi} and elastic - ε_{ei} , Fig.8, a, b. Strain diagrams of the half specimen thickness: a – at the moment of load reached the elastic limit, whole diagram contains elastic component only; b – the plastic

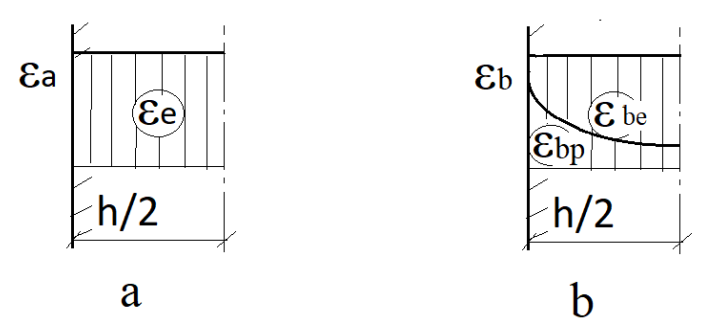


Fig. 8 Relative strain diagram by specimen section, a – elastic part of loading; b – plastic part of loading.

flow beginning from the surface with exponential decreasing to the middle of section, two components of strain in each point of section. With relation of constant load in whole plateau duration, the integral sum of elastic strain by section:

$$\int_0^{h/2} \varepsilon_{be} \, dh = \int_0^{h/2} \varepsilon_e \, dh = \varepsilon_e \times h/2 \quad . \tag{11}$$

From (10) and (11) the sum of plastic strain defined also:

$$\int_0^{h/2} \varepsilon_{bp} \, dh = \varepsilon_b \times h/2 - \varepsilon_e \times h/2 \quad . \tag{12}$$

The comparison of specimens by (12) is possible. The surface value of each may considered as equal. Respectively near surface volume of each with a large share of the plastic flow:

$$h_3 = 3mm; P_3 = (0.513 \times 10^{-2}0) \times 1.5 = 0.77 \times 10^{-2} \ (mm) :$$
 $h_2 = 2mm; P_2 = (0.901 \times 10^{-2}) \times 1 = 0.901 \times 10^{-2} \ (mm) :$ $h_1 = 1mm; P_1 = (1.6 \times 10^{-2}) \times 0.5 = 1.6 \times 10^{-2} \ (mm) .$

Despite a rather big error the values taken from diagram, the trend of P vs h shows, that P seeks to decrease to such minimal constant value when h increase. Otherwise, the ratio of the near surface volume to genera volume increase when

the thickness h decreased. The analysis may be continued with an object-based experiment data.

5.2 Second stage hardening.

First stage hardening ends with the near surface layer formation. It characterized of more stable structure. The plastic strain model as penetration of surface atoms do not contradict to experiments data and all known consequence effects. The moment of the near surface layer saturation characterized of the stress field increasing to the middle of specimen section. The second stage hardening characterized of increasing resistance to strain. The specimen conditions remain the same as at loading start. So, there are no causes for mass transfer direction to change. The most part of volume remain without structural changes. It may be supposed, the only way of plastic flow changes is the group of atoms contemporary displacement from the surface. Such mechanism unrelated to the surface growth and consequently, may lead to the Piobert – Luders effect interruption. Moreover, the PLC (Porteven – Le Chatelier) effect appearance on the second stage hardening may account as natural. The effect appears as serrated load line with – stress drops and peaks. It completely meets the classic form of movement with growing and non-constant resistance. Such plastic flow form has indirect evidence, the localized plastic flow [18].

6 The Problem Formulation.

6.2 Strengthening. The object and methods.

Firstly, it's rational to replace the imprecise term "strength" with functional one – Load Bearing Capacity. The bearing capacity requirements may be classified as variants depend on functionality and desired durability. First – long term resistance to load with low stable strain. Second – the same relation with allowed creep. Third – restricted by time resistance with allowed aftereffect strain. Their

exist some factors else, the common problem may not be formulate. All known methods to increase the strength have a principal restriction. Particularly, metallurgical – alloage and new alloys development in an economy rational cause are restricted by results. Heat treatment – may be applied to alloys and high carbon steels. As sample, bulk hardening is restricted by size of a treated piece. Surface hardening may to consider with special attention. It applied usually for hardness increase. Chemothermal – carburization, nitration, boration, cyanidation. They may be applied for surface hardening. Lasts may to consider also, due to the surface relation changes.

6.3 Formulation.

The ductile metals and alloys take the greatest part in industry and have no restrictions by size in applications. The great treatment experience shows their compatibility to strengthening. It's shown in the project materials the middle part of specimen with sufficient section dimensions may resist to the stresses several times over the proportional limit without irreversible strain. Hence, they are chosen as the object.

The project materials, firstly, the plastic flow model allows to define the problem: development of methods and technique for fixation (the resistance to displacement increasing) of surface atoms. This mean – prevention of the primary plastic changes on the surface.

7 The possible ways to solve.

Some original methods to impact the mechanical properties of metal microstructures was developed by J. Weissmuller and his team, [15,16]. It seems rational to adapt and apply they to the problem to solve.

References.

1. B. Nudelman, Superficial analysis of single crystal at tension (Engineer view)

https://www.nudelman-engineering.com/metal-strength-at-tension

2. N. A. Fleck, G. M. Muller, M. F. Ashby and J. W. Hutchinson, Strain Gradient Plasticity: Theory and Experiment; Acta metall. Mater. Vol 42, No. 2, pp. 475-487, 1994

https://citeseerx.ist.psu.edu/viewdoc/download?doi=10.1.1.613.8544&rep=rep1&type=pdf

3. G SAMBASIVA RAO* and Y V R K "PRASAD, Changes in texture and grain size in hot rolled magnesium and effect on yield strength

Bull. Mater. Sci., Vol. 5, No. 5, December 1983, pp. 459-464

- 4. D. Arola, C.L. Williams Estimating the fatigue stress concentration factor of machined surfaces International Journal of Fatigue 24 (2002) 923–930 https://www.researchgate.net/publication/228980708_Estimating_the_fatigue_st ress_concentration_factor_of_machined_surfaces DOI: 10.1016/S0142-1123(02)00012-9
- 5. Chang Hee Suh, Yun-Chul Jung, and Young Suk Kim, Effects of thickness and surface roughness on mechanical properties of aluminium sheets

Journal of Mechanical Science and Technology October 2010 DOI: 10.1007/s12206-010-0707-7

https://www.researchgate.net/publication/227114876

6. Kye-Man Lee Jieon Park, Sangseok Kim, Sooho Park, and Moo-Young Huh, Quantification of Ridging in Ferritic Stainless Steel Sheets by Electron Backscattered Diffraction R-Value Maps. DOI: 10.1017/S1431927613012245

Microsc. Microanal. 19, S5, 17–20, 2013, at: https://www.researchgate.net/publication/259435522

- 7. Sneddon Scott, Xu Yang, Dixon Mark, Rugg David, Li Peifeng and M. Mulvihill Daniel: Sensitivity of material failure to surface roughness: A study on titanium alloys Ti64 and Ti407, Material and Design, 200, 109438, February 2021
- 8. M. Suraratchai, J. Limido, C. Mabru*, R. Chieragatti Modelling the influence of machined surface roughness on the fatigue life of aluminium alloy International Journal of Fatigue

Volume 30, Issue 12, December 2008, Pages 2119-2126

https://doi.org/10.1016/j.ijfatigue.2008.06.003

https://www.sciencedirect.com/science/article/abs/pii/S0142112308001692

9. Malcolm S Loveday, Tom Gray and Johannes Aegerter: Tensile Testing of Metallic Materials: A Review, 'Competitive and Sustainable Growth' Program, April 2004

- 10. Kolsky, H. (1963) Stress Waves in Solids, Courier Corporation

 https://books.google.co.il/books/about/Stress_Waves_in_Solids.html?id=JRxUj

 BxcpyYC&redir_es
- 11. Vreeland, T., Jr. and Wood, D. S. and Clark, D. S. (1952) A study of the mechanism of the delayed yield phenomenon.

https://authors.library.caltech.edu/54133/

- 12. Yu-Long Cai, Su-Li Yang, Shi-Hua Fu and Qing-Chuan Zhang, The Influence of Specimen Thickness on the Lüders Effect of a 5456 Al-Based Alloy: Experimental Observations, https://www.mdpi.com/2075-4701/6/5/120
- 13. B. Nudelman. Rehbinder Effect, Nudelman Engineering Technology Functional Analysis, Project: Metals Strength at Tension, 2020 http://nudelman-engineering.com
- 14. Wei Wang, Yan Ma, ID, Muxin Yang, Ping Jiang, Fuping Yuan,* and Xiaolei Wu Rate Effect on Tensile Behavior for a High Specific Strength Steel: From Quasi-Static to Intermediate Strain Rates, https://www.mdpi.com/2075-4701/8/1/11
- 15. Hai-Jun Jin and Jörg Weissmüller, A Material with Electrically Tunable Strength and Flow Stress, Science 332, 1179 (2011); DOI: 10.1126/science.1202190

16. Nadiia Mamekaa, Ke Wangb, Jürgen Markmanna,b, Erica T. Lilleoddena and Jörg Weissmüllera, Nanoporous Gold—Testing Macro-scale Samples to Probe Small-scale Mechanical Behavio, Mater. Res. Lett., 2016 Vol. 4, No. 1, 27–36, http://dx.doi.org/10.1080/21663831.2015.1094679

17. E. Cadoni, F. D'Aiuto and C. Albertini, Dynamic behaviour of Advanced High Strength Steels used in the automobile structures; DYMAT 2009 (2009) 135–141 EDP Sciences, 2009 DOI: 10.1051/dymat/2009018

18. С.А. Баранникова, М.В. Надежкин, В.А. Мельничук, Л.Б. Зуев,

О локализации пластической деформации растяжения монокристаллов аустенитной стали, электролитически насыщенных водородом $\mathbb C$; Письма в ЖТФ, 2011, том 37, вып. 17 12 сентября , http://journals.ioffe.ru > articles > viewPDF

B. Nudelman

19.07.2022